

11. HIGH-RESOLUTION, DOWNHOLE, AND NONDESTRUCTIVE CORE MEASUREMENTS FROM SITES 999 AND 1001 IN THE CARIBBEAN SEA: APPLICATION TO THE LATE PALEOCENE THERMAL MAXIMUM¹

Ursula Röhl² and Lewis J. Abrams³

ABSTRACT

Pelagic sediments recording an extreme and short-lived global warming event, the Late Paleocene Thermal Maximum (LPTM), were recovered from Hole 999B (Colombian Basin) and Holes 1001A and 1001B (lower Nicaraguan Rise) in the Caribbean Sea during Ocean Drilling Program Leg 165. The LPTM consists of a 0.3–0.97 m calcareous claystone to claystone horizon. High-resolution downhole logging (Formation MicroScanner [FMS]), standard downhole logs (resistivity, velocity, density, natural gamma ray, and geochemical log), and non-destructive chemical and physical property (multisensor core logger [MSCL] and X-ray fluorescence [XRF] core scanner) data were used to identify composite sections from parallel holes and to record sedimentological and environmental changes associated with the LPTM.

Downhole logging data indicate an abrupt and distinct difference in physical and chemical properties that extend for tens of meters above and below the LPTM. These observations indicate a rapid environmental change at the LPTM, which persists beyond the LPTM anomaly. Comparisons of gamma-ray attenuation porosity evaluator (GRAPE) densities from MSCL logging on split cores with FMS resistivity values allows core-to-log correlation with a high degree of accuracy. High-resolution magnetic susceptibility measurements of the cores are compared with elemental concentrations (e.g., Fe, Ca) analyzed by high-resolution XRF scanning.

The high-resolution data obtained from several detailed core and downhole logging methods are the key to the construction of composite sections, the correlation of both adjacent holes and distant sites, and core-log integration. These continuous-depth series reveal the LPTM as a multiphase event with a nearly instantaneous onset, followed by a much different set of physical and chemical conditions of short duration, succeeded by a longer transition to a new, more permanent set of environmental circumstances. The estimated duration of these “phases” are consistent with paleontological and isotopic studies of the LPTM.

INTRODUCTION AND BACKGROUND

To infer paleoceanographic information from physical and chemical characteristics of sediment it is necessary to obtain the most continuous and accurate measurements possible. Standard analytical methods for discrete samples are noncontinuous, time consuming, and expensive. Relatively fast core logging methods and certain high-resolution downhole measurements can now obtain continuous data at much finer scales (down to millimeter scale) than are practical for individual sampling methods. In addition, logging methods are nondestructive and, in the case of downhole measurements, record data continuously over nonrecovered and recovered intervals of the borehole. These enormous advantages are important for the relatively long Ocean Drilling Program (ODP) cores and especially for critical boundaries, which were major objectives of Leg 165 (Fig. 1A).

One especially interesting and important paleoceanographic episode sampled at two sites during Leg 165 is known as the Late Paleocene Thermal Maximum (LPTM) (Kennett and Stott, 1991; Zachos et al., 1993), which occurred approximately 55 Ma in the late Paleocene Epoch. Figure 1B shows the location of drill sites in the Caribbean of the Paleocene. The LPTM represents a relatively short but most pronounced event of global warming and is associated with dramatic changes in the biosphere and ocean circulation. Oxygen isotope records indicate a rapid (<10 k.y.) warming of high-latitude surface and deep waters (Kennett and Stott, 1991; Shackleton, 1986; Zachos

et al., 1993). The large negative excursion of $\delta^{18}\text{O}$ is coeval with a large, short-term decrease in $\delta^{13}\text{C}$ in both marine and terrestrial records and a major global extinction of benthic foraminifers (Kennett and Stott, 1991; Pak and Miller, 1992; Thomas and Shackleton, 1996). The event is believed to have been associated with a temporary change in dominant deep-water sources from high to low latitudes (Pak and Miller, 1992; Eldholm and Thomas, 1993). The resulting decrease in dissolved oxygen content of warmer deep waters is likely the major cause of the mass extinction of benthic foraminifers (Kennett and Stott, 1990, 1991; Thomas and Shackleton, 1996). Isotope excursions and the benthic faunal extinction occurred rapidly (<10⁵ yr) (Kennett and Stott, 1991; Aubry et al., 1996), and isotope values and species richness returned to pre-excursion levels in ~50,000 yr (Kennett and Stott, 1991; Thomas and Shackleton, 1996). Prior to Leg 165, sediments documenting the LPTM were identified in deep sea sequences of the Southern Oceans (Kennett and Stott, 1991), the Indian Ocean (Zachos et al., 1992), the equatorial Pacific (Bralower et al., 1995), and the Atlantic (Pak and Miller, 1992; Thomas and Shackleton, 1996).

The long-term warming of the late Paleocene climate may be related to elevated levels of atmospheric CO₂, perhaps caused by the voluminous CO₂ degassing of the effusive eruptions from the North Atlantic igneous province (Eldholm and Thomas, 1993). However, it appears that only high latitudes warmed significantly, whereas equatorial areas remained at much the same temperature as today (Shackleton and Boersma, 1981; Bralower et al., 1995). Bralower et al. (1997) proposed that a circum-Caribbean volcanic episode, documented by abundant ash layers found interbedded within rocks containing the LPTM layer of Sites 999 and 1001, may have resulted in short-term atmospheric cooling preferentially at low latitudes. This preferential cooling at low latitudes would act to decrease the difference between high- and low-latitude sea-surface temperatures (SSTs), perhaps triggering a change of deep-water sources from high-

¹Leckie, R.M., Sigurdsson, H., Acton, G.D., and Draper, G. (Eds.), 2000. *Proc. ODP, Sci. Results*, 165: College Station, TX (Ocean Drilling Program).

²Geosciences Department, Bremen University, P.O. Box 33 04 40, D-28334 Bremen, Federal Republic of Germany. uroehl@allgeo.uni-bremen.de

³Department of Earth Sciences, University of North Carolina at Wilmington, 601 South College Road, Wilmington, NC 28403-3297 U.S.A.

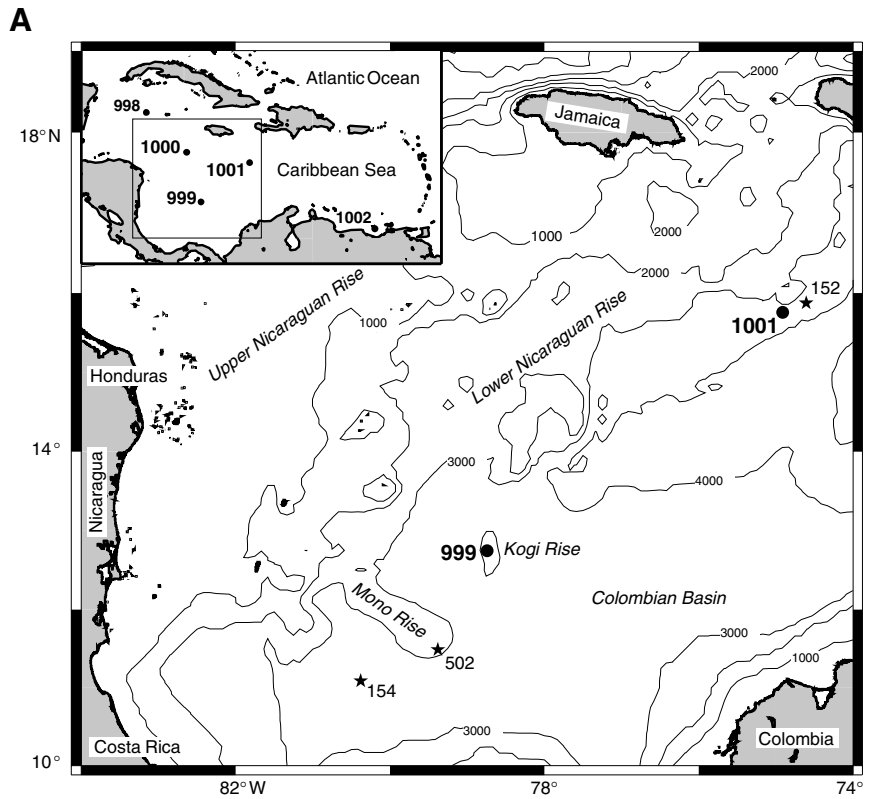


Figure 1. A. ODP Sites 999 and 1001 (solid circles) and nearby DSDP sites (stars). Boxed insert shows location of all sites drilled during Leg 165 in the Caribbean Sea. Contours are in meters below sea level (GMT map, Wesel and Smith, 1995).

to low-latitude areas. The consequent warming of deep water could have resulted in the dissociation of gas hydrates, fueling further climatic warming and the dramatic transformation within the global carbon cycle, as characterized by the large negative $\delta^{13}\text{C}$ excursion at the LPTM (Dickens et al., 1995, 1997).

In this paper we demonstrate that our data uniquely defines the lithologic, physical, and chemical properties across the two Caribbean LPTM sections by continuous downhole logging and shore-based measurements of gamma-ray attenuation porosity evaluator (GRAPE) density, magnetic susceptibility, and chemical intensities of the cores by different core scanning (i.e., core logging) methods.

There are a number of core logging methods that are now routinely utilized both aboard the *JOIDES Resolution* and in shore-based laboratories, such as Minolta™ color scanning and physical properties logged by a multisensor track (MST) (e.g., Curry et al., 1995; Sigurdsson, Leckie, Acton, et al., 1997). These types of conventional continuous core-log methods indirectly define parameters which are important for paleoceanographic interpretations (e.g., carbonate contents are derived from color data, sediment densities are calculated from attenuation of gamma-rays, terrigenous input is interpreted by variations in the magnetic susceptibility).

In addition to standard logging methods of cores and in the borehole, we applied a relatively new method of geochemical core logging. In contrast to conventional core log measurements, the X-ray fluorescence (XRF) core scanner is able to directly measure several parameters that are important for paleoceanographic interpretations, such as Ca (representing “carbonate”) and Fe (representing “terrigenous” and/or “volcanic”). The XRF core scanner measurements are not affected by the length of time since the core was cut, which can affect color measurements, and/or reduction diagenesis within the core, which can alter magnetic susceptibility. These are factors that can have an enormous influence on the quality and continuity of conventional core log data and, therefore, limit paleoceanographic interpretation.

Continuous rotary coring rarely results in continuous core recovery, and Leg 165 drilling was no exception. Downhole measurements

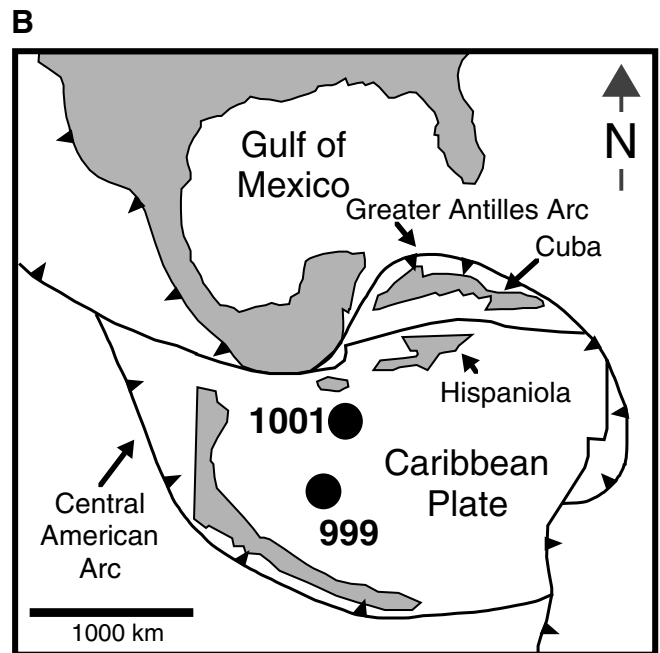


Figure 1 (continued). B. The Paleocene Caribbean (tectonic reconstruction from Pindell and Barrett, 1990) and location of Sites 999 and 1001.

still provide the only continuous record of the borehole wall. We will show that detailed correlation of high-resolution downhole measurements and continuous core log data allow exact core log integration. The creation of composite sections was essential for sampling plans to verify and define the LPTM by its typical negative shift in carbon isotope values (Bralower et al., 1997), and the correlation of both adjacent holes and distant sites. Furthermore, the data provide thickness

estimates of the LPTM claystone, time estimates of the onset and duration of the LPTM, and constraints on the occurrence and distribution of associated ash layers. Together these observations further define the dramatic oceanographic, climatic, and paleoenvironmental changes associated with the LPTM event.

METHODS

Core Logging

We used continuous measurements of physical properties of the cores: the MST aboard *JOIDES Resolution* (Sigurdsson, Leckie, Acton, et al., 1997) and the split core multisensor core logger (MSCL, GEOTEK™, Surrey, UK; Weaver and Schultheiss, 1990; Gunn and Best, 1998) from the Geosciences Department of Bremen University, which we temporarily took to the Bremen ODP repository. The MSCL includes instruments that measure magnetic susceptibility and density. Magnetic susceptibility data were collected at 1 cm intervals using a Bartington™ point sensor, which is more accurate for measuring half cores and gives much higher spatial resolution than the loop sensor. Densities were also determined from GRAPE measurements recorded at 1 cm intervals (Boyce, 1976).

Shipboard GRAPE density values (obtained by MST) do not match the magnitude of the shipboard wet bulk density data (index properties of individual samples) below 400 meters below seafloor (mbsf) at Site 999 (Sigurdsson, Leckie, Acton, et al., 1997). The cores at these depths do not fill the liner because of the increased induration of the sediments. The gamma-ray attenuation processing aboard ship assumed a core diameter corresponding to a filled liner; therefore, the resulting GRAPE density values are too low (Sigurdsson, Leckie, Acton, et al., 1997). In order to compare shore-based and shipboard GRAPE measurements, the shore-based GRAPE density values are normalized to the shipboard GRAPE density data.

The chemical element composition of the cored material was analyzed using a new XRF core scanner. The XRF core scanner is a non-destructive analysis system for scanning the surface of archive halves of cores. The instrument was developed and built at the Netherlands Institute for Sea Research (NIOZ, Texel). The general method and some calibration procedures are described by Jansen et al. (1998).

Here we present the specifications and procedures of the system at the Geosciences Department of Bremen University and how we adapted it to the LPTM cores. The XRF core scanner is installed within a standard 20-ft container to allow easy transport. Both the cover and the core fit system are pneumatically activated. The central sensor unit consists of a molybdenum X-ray source (3–50 kV) and a Peltier-cooled PSI detector (KEVEX™) with a 125 μm beryllium window and a multichannel analyzer with a 20 eV spectral resolution (Fig. 2). The whole system is computer controlled. The scanner electronics allow precise positioning capabilities and include an integrated safety interlock mechanism. Our system configuration (X-ray tube energy, detector sensibility) allows the analysis of elements from potassium (K, atomic number 19) through strontium (Sr, atomic number 38; 20 kV X-ray voltage). The analyses are performed at predetermined positions and counting times. The measurement unit (X-ray source, detector) is moved along the Z axis, the plastic prism is lowered on the core surface (covered by special foil) during analysis; a slit defines the dimensions of the irradiated core surface (here: 1 cm^2). To avoid loss of energy because of scattering in air, the area of analysis is flushed by helium (between prism and detector, covered by a condom, and within the prism). The core is moved along the X axis (Fig. 2). The XRF data are collected at 1 cm intervals over a 1 cm^2 area, and test run calibration resulted in the use of 15 s count time and an X-ray current of 0.15 mA to obtain statistically significant data of the elements we were interested in (e.g., K, Ca, Fe, Ti, Mn, Sr). In this paper we present Ca and Fe intensity data, which are highly correlated to the physical and chemical properties measured both downhole and

in cores. The relatively indurated LPTM cores were cut by a saw, and therefore, already had an ideally flat core surface, which is needed for successful XRF analysis. Most of the rotary-drilled cores are broken into several centimeter to decimeter long pieces. Special effort was taken in preparing the cores carefully by bringing all the single pieces up to one level. The response of the elements also depends on the wavelength of the fluorescent radiation; the penetration depth of the XRF analysis is on the order of tenths of millimeters (Ca) and hundredths of millimeters (Fe) deep. Therefore, special accuracy was needed for cleaning cutting residues from the core surface. The acquired XRF spectrum for each measurement is processed by the KEVEX™ software Toolbox®. Background subtraction, sum-peak and escape-peak correction, deconvolution, and peak integration are successively applied. The resulting data are basically element intensities in counts per second. Element concentrations (e.g., in percent or parts per million) are not directly available, but by comparisons with data from standard chemical analyses from discrete samples, these counts can be converted to element concentrations (Jansen et al., 1998).

Downhole Logging Data

Downhole logging measurements of the borehole wall at Sites 999 and 1001 were accomplished by a suite of different instruments including the long-spaced sonic tool (sonic velocity), natural gamma-ray tool (natural gamma-ray activity), lithodensity tool (bulk density), the dual induction–spherically focused resistivity tool (three different measurements of resistivity), and the FMS tool (described below). In addition, dry weight fractions of major oxides were derived at Site 999 using data from the geochemical tool, and at Site 1001, magnetic polarity reversals were obtained using data from the geological high-sensitivity magnetic tool. A complete description of individual logging instruments is given in the *Ocean Drilling Program Manual* (Borehole Research Group, 1990) and in Sigurdsson, Leckie, Acton, et al. (1997), for Leg 165 downhole measurements in particular. FMS data and data processing are detailed below because of the introduction of “calibrated” FMS data and the importance of FMS data to core log integration.

The FMS produces high-resolution images of the resistivity character of the borehole wall that can be used for detailed sedimentological and/or structural interpretations (Ekstrom et al., 1986; Bourke et al., 1989; deMenocal et al., 1992). The FMS tool comprises 16 electrode “buttons” on four orthogonal pads that are pressed against the borehole wall. The electrodes are spaced 2.5 mm apart and are arranged in two diagonally offset rows of eight electrodes each. A

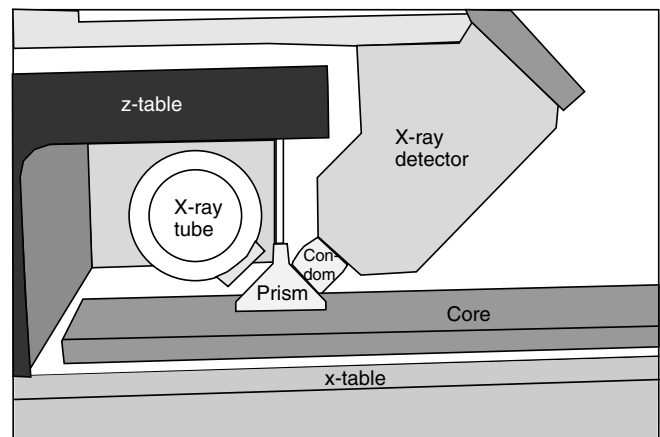


Figure 2. View into the measurement chamber of the XRF core scanner of the Geosciences Department of Bremen University. The X-ray tube and the detector are oriented so that the incident beam and the detector make an angle of 45° with the surface of the sample.

focused electrical current flows between electrodes and variations in current intensity are measured. These measurements reflect resistivity variations, are recorded every 0.25 cm, have a 0.5 cm vertical resolution, and have a maximum penetration depth of 25 cm. In contrast, conventional downhole measurements are recorded every 15 cm and have vertical resolutions ranging from 15 cm to 2 m (deMenocal et al., 1992). Thus, the sampling rate for FMS is 60 times greater than conventional logs, with resolution capabilities 30–400 times greater than conventional logs. This fine-scale resolution makes FMS the downhole measurement that is most comparable in scale to measurements made on whole core and individual samples, as well as providing visual comparisons to core photographs.

The FMS tool string contains a general purpose inclinometry tool (GPIT) that orients the measurements relative to magnetic north through the use of a magnetometer and records variation in uphole speed through the use of an accelerometer. Standard processing utilizes information from the GPIT and converts variations in current intensity as recorded on 16 individual electrodes on each pad into spatially oriented, variable-intensity color or gray-scale images of the borehole wall. The FMS images reveal relative variations in borehole resistivity but do not provide a direct quantitative value of formation resistivity.

Resistivity in this environment is primarily controlled by electrolytic conduction of pore fluids and/or cation exchange on the surfaces of clays and other conductive minerals (Bourke et al., 1989). Thus, images of resistivity variations reflect changing chemical and physical properties of the borehole such as porosity, mineralogy, induration, grain size, and chemistry of pore fluids.

The standard presentation of FMS data as variable-intensity gray-scale images are often visually similar to split cores or black and white photographs of the cores. Although visual correlations can be striking, they can not easily be quantitatively interpreted. In addition, all other core measurements are presented as a digital depth series of discrete data values, which are not always easily correlated to gray-scale images. In order to expand the use of FMS data as a link between core and all other discrete measurements, FMS relative resistivities are scaled to the absolute resistivity measured with the shallow spherically focused resistivity log (SFLU), and a digital depth series of scaled FMS resistivity values are extracted.

Scaling of FMS data to measurements of absolute formation resistivity was accomplished at the Laboratoire de Mesures en Forage, IMT, Marseille, France, using the proprietary Schlumberger™ software module known as “BORSCA®.” Scaled FMS data are displayed as a single “wigggle” trace of resistivity (ohm-m) with depth calculated every 1.27 cm, and represent the sum of scaled values from 16 electrodes on one of four orthogonal pads. This electrode averaging and use of one pad is appropriate given the flat-lying strata imaged with the FMS in the depth intervals discussed in this paper. Scaled (calibrated) FMS data are compared to “raw” FMS data over the same depth interval in Figure 3.

The images from four tool pads cover ~22% of the borehole wall for each pass; however, the FMS images presented in this paper are shifted closer together for display purposes and thus appear to cover a greater percentage of the borehole (e.g., Figs. 4, 5, 6). Calipers on the FMS tool provide precise measurements of borehole diameter in two orthogonal directions. Use of the FMS is restricted to hole diameters <38 cm (15 in). All depth intervals presented in this study have hole diameters between 28 and 35 cm.

FMS data in this paper are displayed as a combination of standard gray-scale images and the calibrated trace from one of four pads. In the gray-scale FMS images, black represents the least resistive values and white the most resistive ones. For the cores examined in this paper; calcareous horizons are characterized in the image by light gray to white; intermediate grays reflect calcareous–clayey mixed sediments; distinct volcanic ash layers show up as dark gray to black sharp-bounded thin layers, and clay-rich intervals (not necessarily

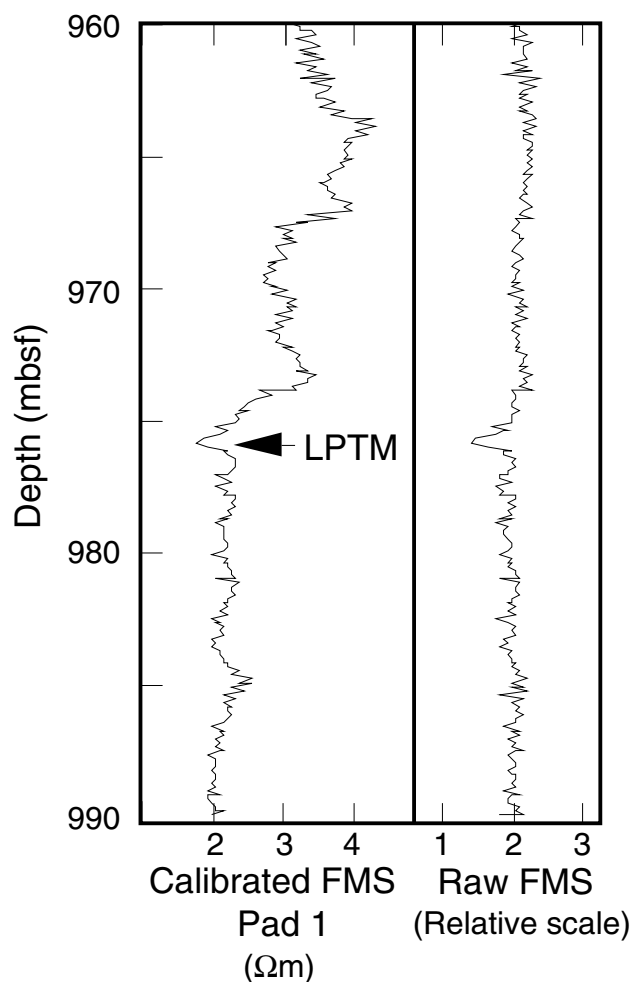


Figure 3. Comparison of calibrated vs. uncalibrated (raw) FMS data from Site 999. Each trace represents the average from the 16 button electrodes on Pad 1. Calibration method is described in text.

altered ash) are also characterized by black, low resistivity intervals. Disseminated chert and/or zones of silicification may also be evident as irregularly shaped white areas. The FMS trace acts as a visual “link” between the FMS image and all other downhole and core measurements, which are also presented as discrete values with depth. The FMS data play an important role in reconstructing the sequences with incomplete recovery.

Depth Shifting

Depths for downhole measurements data are initially determined by the length of wire suspended below the rig floor adjusted for the position of a particular tool on the tool string. Wireline length is then calibrated to the position of the end of the drill pipe, which is at a known depth below the dual-elevator stool on the rig floor, which in turn, is at a measured elevation above mean sea level. The “bottom felt depth” representing the first contact of the drill string with sea-floor is used to convert core and log depths to mbsf. Downhole measurements made during different trips into the open hole are depth calibrated to each other using a natural gamma-ray spectrometry tool (NGT), which is included on every tool string, including the FMS, as a common correlative measurement. Downhole measurements presented in this paper are those found on the CD-ROM in Sigurdsson, Leckie, Acton, et al. (1997), which have been depth shifted by the

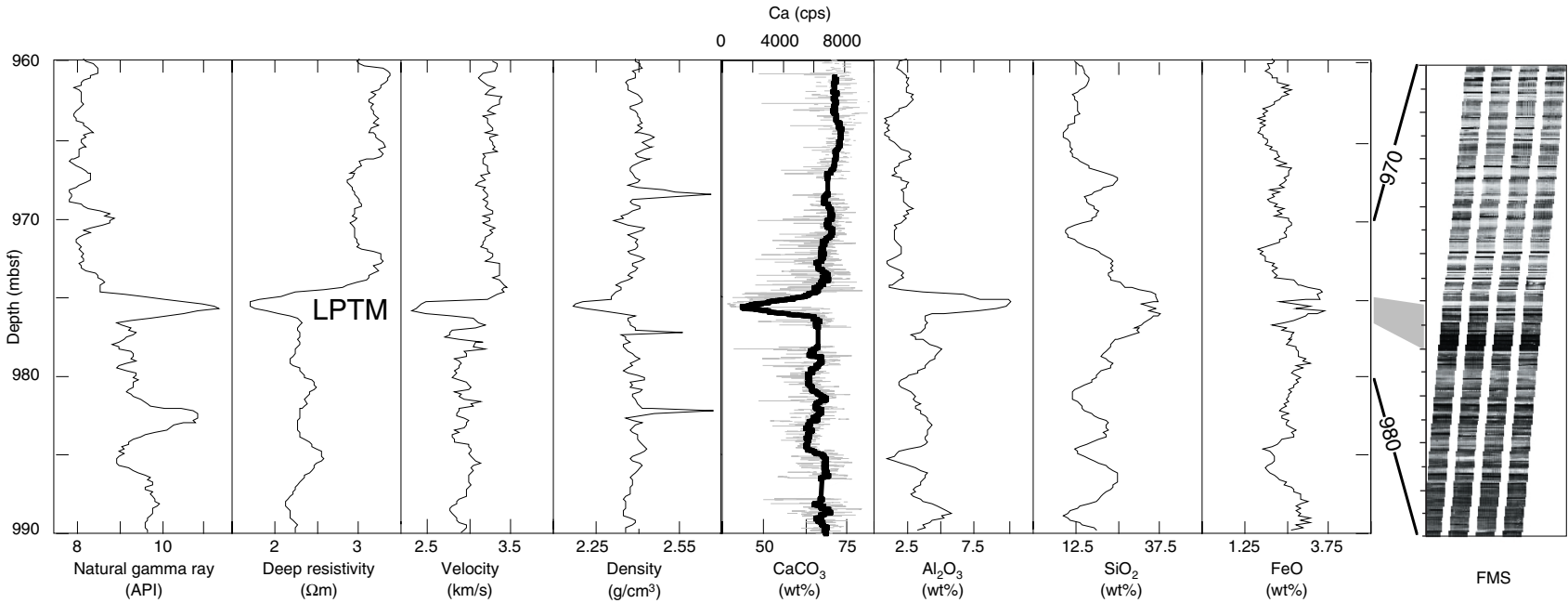


Figure 4. Late Paleocene thermal maximum (LPTM) as observed in a variety of downhole measurements at Site 999. The log response at 975.5 mbsf is consistent with the recovered claystone interval that contains the negative $\delta^{13}\text{C}$ excursion marking the LPTM. These data indicate an abrupt and distinct difference in physical/chemical properties that extend for tens of meters above and below the LPTM. The variation in CaCO_3 concentration as derived from measurements made with the downhole geochemical tool compares well with that of Ca concentration measured with the XRF core scanner (thick line), and both indicate the dramatic decrease in carbonate at the LPTM.

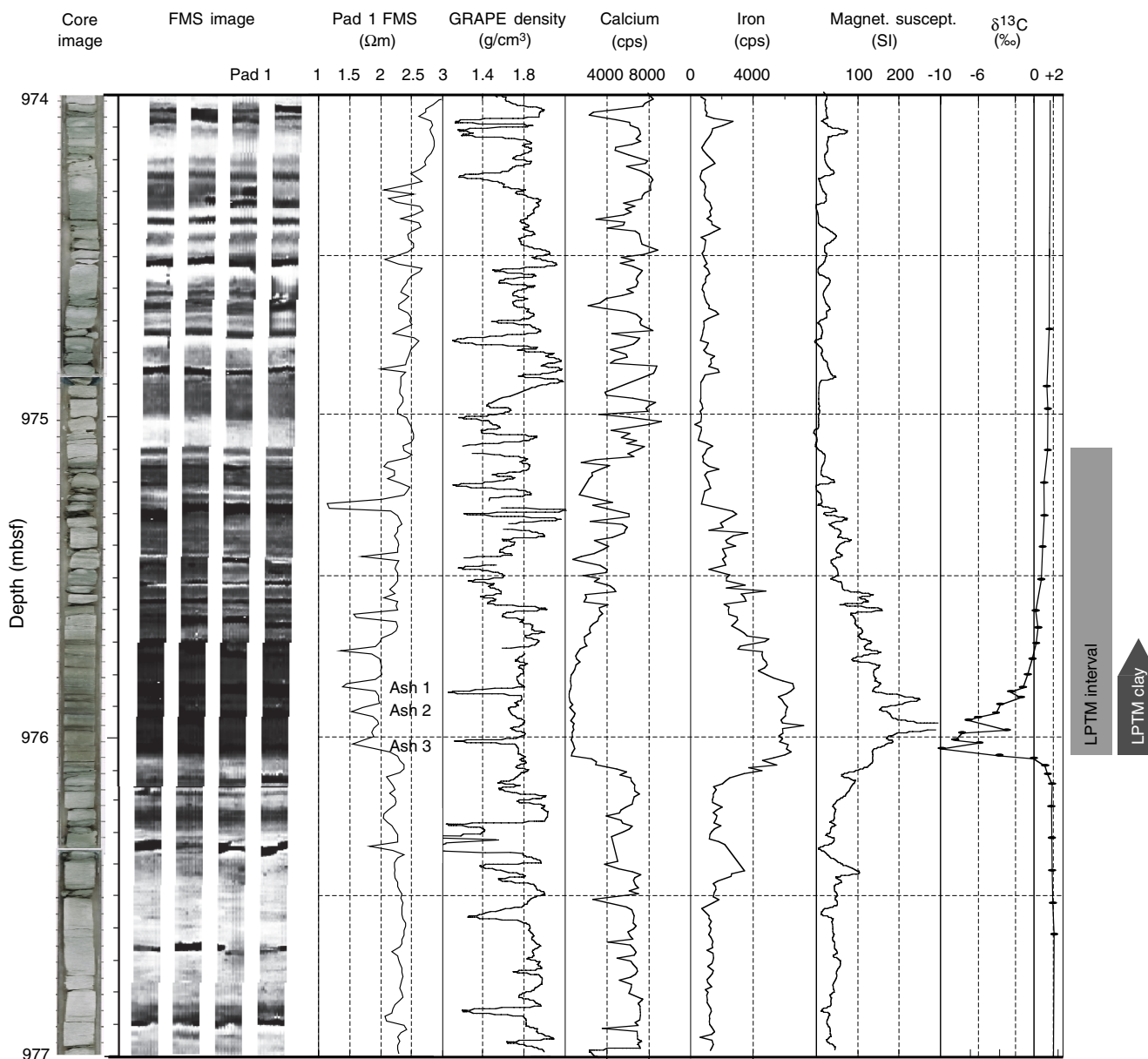


Figure 5. The upper Paleocene interval drilled in Hole 999B. The section from 974 to 977 mbsf (logging depth) is shown next to the core image. The carbon isotope curve (from Bralower et al., 1997) identifies the LPTM by its typical negative carbon isotope excursion. All core logging data from the MSCL and XRF core scanner are collected in 1 cm steps.

Lamont-Doherty Earth Observatory Borehole Research Group (LDEO-BRG). Regardless of the absolute depth value, relative thicknesses and spacing of features displayed on FMS and other downhole measurements should be identical within the limits of varying vertical resolution capabilities.

Although both core and log depth values are given relative to drill-string measurements, numerous factors including incomplete core recovery result in depth mismatches between core and downhole measurements. Depths (mbsf) given in this paper are from the FMS tool string; thus, where depth discrepancies are found, core depths are shifted to match FMS downhole measurements.

SELECTED SITES

The LPTM interval was recovered at Site 999 (Kogi Rise in the Colombian Basin) and Site 1001 (lower Nicaraguan Rise) (Fig. 1A).

The crest of the Kogi Rise at 2800 m water depth lies ~1000 m above the turbidite-laden floor of the Colombian Basin. A complete, almost 1067-m-thick sequence of largely pelagic/hemipelagic sediments from the Maastrichtian to the Pleistocene was recovered at Site 999 (Sigurdsson, Leckie, Acton, et al., 1997). Upper Paleocene and lower to middle Eocene sediments consist of clayey calcareous limestones, clayey calcareous mixed sedimentary rocks with some interbedded ash layers, and nearly pure claystones. The sediments are slightly to moderately bioturbated. Only a few millimeter-thick volcanic ash layers were identified. Sedimentation rate at Site 999 is 32.2 m/m.y. over the interval that includes the LPTM (Sigurdsson, Leckie, Acton, et al., 1997).

Site 1001 is located on the lower Nicaraguan Rise in 3259 m water depth. The Neogene cap is thin, and a continuous Paleocene to Upper Cretaceous sequence was recovered from 165 to 485 mbsf. The upper Paleocene to middle Eocene sediments are primarily composed of calcareous chalk with foraminifers and mixed sedimentary rocks

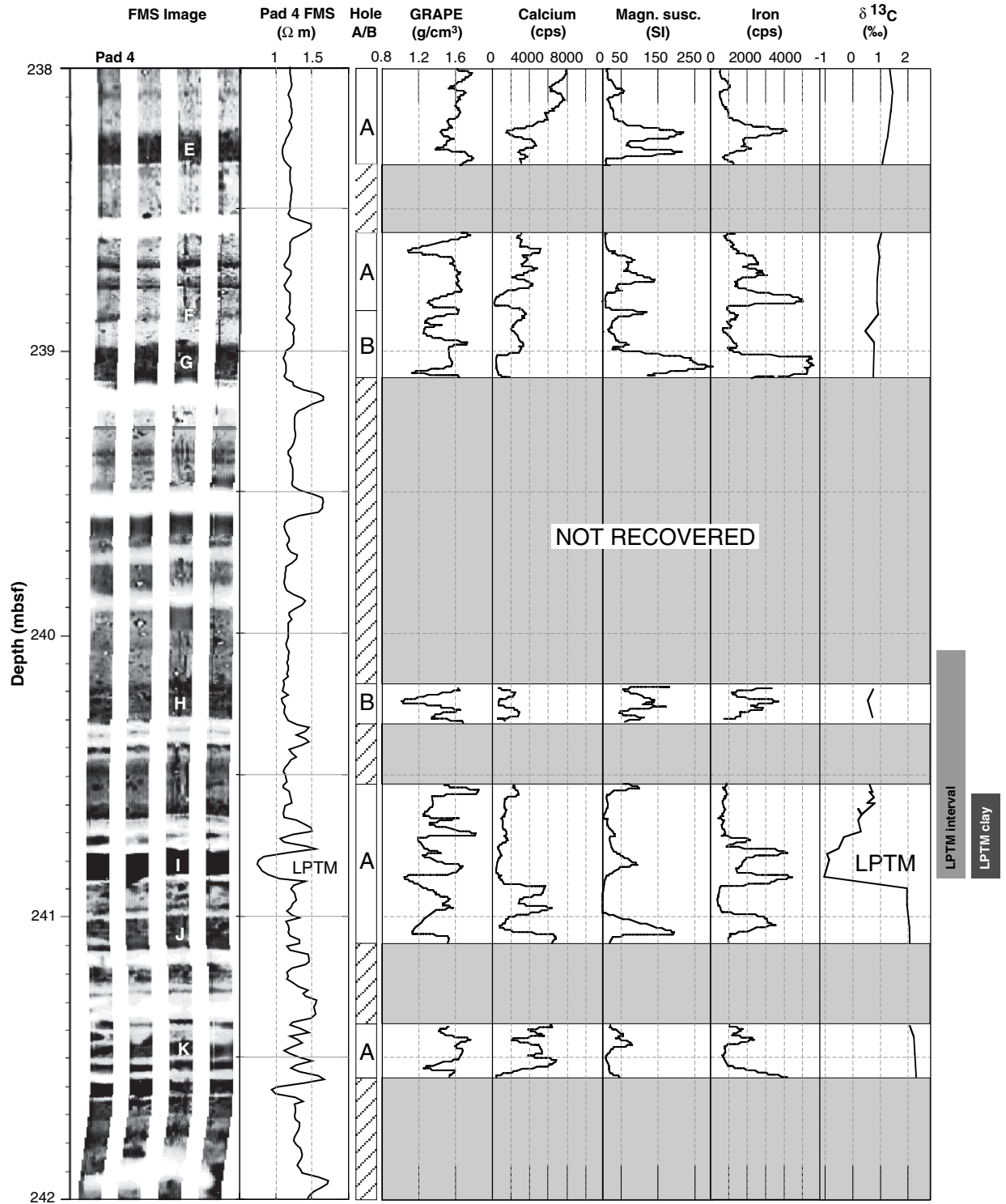


Figure 6. The composite upper Paleocene interval recovered at Site 1001 as a result of detailed correlation between the core data of the two adjacent holes 1001A and 1001B and comparison with continuous downhole FMS data. The section from 238 to 242 mbsf (logging depth) is shown. In the FMS image the white letters indicate volcanic ash layers used for correlation (modified from Bralower et al. [1997]). The carbon isotope curve (from Bralower et al. [1997]) identifies the LPTM by its typical negative carbon isotope excursion. All core logging data from the MSCL and XRF core scanner are collected in 1 cm steps.

with clay and minor chert and volcanic ash layers. Sedimentation rate for the latest Paleocene and earliest Eocene interval is 37.4 m/m.y. (Sigurdsson, Leckie, Acton, et al., 1997). The upper Paleocene sediments at Site 1001 are characterized by more pronounced pure limestone or claystone end members, whereas at Site 999, the sediments are generally dominated by the mixed clayey calcareous sediment types and pure end members are less represented.

Benthic foraminifer assemblages indicate a lower-bathyal to upper-abyssal (1500–2500 m) late Paleocene water depth for Site 999; and Site 1001 was toward the lower end of this range. Paleomagnetic studies indicate that both sites were closer to the equator in the late Paleocene (~10°N) (Sigurdsson, Leckie, Acton, et al., 1997; Acton et al., Chap. 9, this volume) and Site 999 was more proximal to the Central American Arc (Fig. 1B).

These sites provide a unique data set for examining lithologic variability around the LPTM and the relationship to physical and chemical properties determined by logging. Prior to Legs 165 and 171B the majority of drill sites penetrating upper Paleocene sections either did not obtain any downhole logging data (e.g., Sites 690 and 865) or very limited downhole data in high latitude and shallow marine environments. For example, only natural gamma-ray downhole logs for the Paleocene–Eocene interval were described for a well in the North Sea by Knox (1996) and Neal (1996). In contrast to most other deep-sea sites sampling this interval, sediments and logs obtained from Holes 999B, 1001A, and 1001B provide a complete record of the LPTM, and along with Site 865 in the Western Pacific and Leg 171B sites in the Western Atlantic, also provide relatively rare high-resolution records of low-latitude deep-sea Paleogene stratigraphy (e.g., Bralower et al., 1995; Norris, Kroon, Klaus, et al., 1998).

Because of the relatively wide lithologic range consisting of the end members: nannofossil foraminifer limestones, clays, and volcanic ashes, and in combination with the incomplete recovery, we undertook a high-resolution investigation of physical and chemical properties of both the recovered cores and of the borehole wall using standard and high-resolution downhole logs. The LPTM interval in the cores of Holes 999B, 1001A, and 1001B consists of 0.3–0.97-m-thick clay-rich horizons with significantly lower carbonate contents compared to the surrounding chalks, limestones, and clayey calcareous mixed sediments with some ash layers (Sigurdsson, Leckie, Acton, et al., 1997). Because of the high burial depth (~975 mbsf), the LPTM cores of Hole 999B are relatively lithified (porosity of 22%–27.5%, *P*-wave velocity of 3.1–3.5 km/s) and contain less water (8.5–11.8 wt% water). The LPTM Cores 165-1001A-27R and 165-1001B-6R, drilled on the Lower Nicaraguan Rise at 235–242 mbsf, contain 25–31 wt% water and still have 50%–61% porosity (Sigurdsson, Leckie, Acton, et al., 1997).

RESULTS

Site 999

Downhole Measurements

Downhole measurements reveal a distinct anomaly centered at ~975.5 mbsf, which consists of local maxima in total gamma-ray counts, SiO₂, Al₂O₃, and FeO, with local minima in sonic velocity, density, resistivity, and CaCO₃ values (Fig. 4). These co-varying extreme logging values extend for less than a meter. There is also a distinct change in mean log values below and above the anomaly (e.g., natural gamma ray, resistivity, velocity, Al₂O₃). This abrupt change in logging values extends uniformly for 10–15 m above and below the anomaly.

The FMS image reveals a 97-cm-thick interval (975.09–976.06 mbsf; Figs. 4, 5) of relatively low resistivities (dark gray–black). The anomaly in standard downhole logs is centered on this interval

(~975.5 mbsf; Fig. 4). The darkest area (lowest resistivity) in the FMS image from 975.69 to 976.06 mbsf (37 cm thick) lies at the base of this generally low resistivity zone.

The calibrated FMS resistivity curve reveals a 1.5–2.0 m transition zone between the minimum resistivity values (<2 ohm-m) at the log anomaly, which grade up to greater than 3.0 ohm-m at ~974 mbsf without returning to pre-anomaly values (Fig. 5). The calibrated FMS resistivity curve also shows four distinct minima within the 37-cm-thick, low resistivity zone.

Core Logs

Two characteristic low GRAPE density peaks were identified at 975.85 and 976.02 mbsf within a narrow zone of nearly constant density from 975.6 to 976.25 mbsf (Fig. 5). The density values above and below this zone show much more variability, especially the overlying interval.

The calcium intensities (in cps) reflect the relative variation of this element. The Ca intensities are relatively constant from 976.06 to 977 mbsf. An abrupt decrease is at 976.05 mbsf, and a transitional zone back to higher values starts at 975.8 mbsf (Fig. 5). Both the GRAPE density data and the Ca intensities are more variable above 975.6 mbsf than below 976.2 mbsf. The iron intensities (Fe, cps) are negatively correlated to the calcium values. Between 976.06 and 977 mbsf there are more variations in the Fe intensities than within the interval characterized by low-Ca intensities. Three Fe intensity peaks are at 975.85, 975.94, and 976.05 mbsf; the sharp peak at 975.94 mbsf is the most prominent one. The magnetic susceptibility values generally correlate well with the Fe intensities (Fig. 5). Sharp peaks are easy to identify at 975.94 and 976.05 mbsf.

Core Log Integration and Interpretation

The correlation of core data to downhole measurements is essential for holes with incomplete recovery. Fortunately, at Site 999 more than three quarters of the drilled hole is represented by cores (76.1% overall and 87.7% over the LPTM interval). Log-to-core correlations for the LPTM interval at Site 999 are most easily obtained by first matching the general character of the largest anomaly in the data from downhole measurements to core-log measurements and interpreting the logging response in terms of varying lithology and porosity.

The co-varying, extreme downhole logging values that extend for less than a meter at ~975.5 mbsf (Fig. 4) are indicative of a much less indurated zone with relatively high clay content. A significant anomaly is also apparent in the core log data. The minimum in Ca counts correspond to maxima in Fe counts and magnetic susceptibility. This response is also indicative of a carbonate-poor, clay-rich interval (original core depth = 975.23–975.65 mbsf). It is clear that there is a dramatic anomaly in measurements common to both downhole and core logs (e.g., CaCO₃ vs. Ca, FeO vs. Fe; Fig. 4) as well as co-varying measurements (e.g., high Fe counts and gamma-ray counts both responding to increased clay content). The nearly identical match in downhole log depth and core depth makes this an unequivocal correlation. In general, all these logging responses are consistent with the recovery of a claystone layer (975.15–975.7 mbsf core depth) within bioturbated, clayey, calcareous, mixed sediment (Sigurdsson, Leckie, Acton, et al., 1997).

Both the core logs and downhole logs show that an abrupt lithologic, physical, and chemical transition occurred in association with the recovered claystone. The identification of this claystone as the LPTM claystone is confirmed by shipboard biostratigraphy and, more critically, by the distinct negative $\delta^{13}\text{C}$ excursion that characterizes the LPTM at other drill sites worldwide (Bralower et al., 1997). The LPTM claystone (or LPTM clay) is defined as the interval containing the anomalous $\delta^{13}\text{C}$ minima. The $\delta^{13}\text{C}$ anomaly has an abrupt

onset as it does at other sites, and this marks the base of the LPTM clay. The depth of the LPTM clay base is most accurately determined by the FMS in cases where recovery is not 100% and is well defined at 976.06 mbsf by the abrupt onset of low resistivities (Figs. 4, 5). Thus, core log depths are shifted by 40 cm to align the onset of core log anomalies (e.g., Ca, Fe) and the $\delta^{13}\text{C}$ anomaly to the base of the FMS-defined LPTM claystone interval.

The generally good correlation between GRAPE density, carbonate content (Ca, cps), and high FMS resistivity reflects more indurated, less porous nature of the higher carbonate sediment. In contrast, the correlation of iron intensities, magnetic susceptibility, and lower FMS resistivity characterizes the relatively soft, highly porous, clayey sediments with relatively high amounts of pore water.

The LPTM anomaly in standard downhole logs is centered on the 97-cm-thick zone (975.09–976.06 mbsf, Fig. 5) of relatively low FMS resistivity, and encompasses the 55-cm-thick claystone recovered in core interval 165-999B-51R-5, 75–150 cm (Sigurdsson, Leckie, Acton, et al., 1997). In addition, XRF Ca and Fe counts remain both below and above pre-LPTM levels throughout this interval, respectively. The darkest area (lowest resistivity) in the FMS image from 975.69 to 976.06 mbsf (37 cm thick) lies at the base of this generally low-resistivity zone and correlates to the negative $\delta^{13}\text{C}$ excursion, Ca minimum, Fe and magnetic susceptibility maximum, and an interval of less variable GRAPE density values (Fig. 5).

The nearly constant minimum Ca intensities and maximum Fe intensities, as well as the extreme $\delta^{13}\text{C}$ values extend over an ~25 cm interval. Thus, we define the thickness of the LPTM clay as 25–37 cm at the base of a broader region (97 cm) referred to as the LPTM interval where carbonate content remains relatively low. The LPTM consists of a greenish gray, partly fine-laminated claystone (see core image, Fig. 5). Comparison with shipboard carbonate data obtained from analyses of discrete samples (Sigurdsson, Leckie, Acton, et al., 1997 and Bralower et al., 1997) with measured Ca intensity variations of ~200 to >8000 cps reflect carbonate contents from <0.5% (in the LPTM clay) to up to 68% CaCO_3 (in the post-LPTM interval). The abrupt onset of the FMS resistivity anomaly followed by a tran-

sition zone is similar to the pattern displayed by Ca, Fe, and magnetic susceptibility values (Figs. 4, 5).

Macroscopically we identified three mm-thick ash layers within the LPTM clay (layers “Ash 1” to “Ash 3” in fig. 5 of Bralower et al., 1997). The calibrated FMS resistivity curve shows four distinct minima within the LPTM claystone. Three of these minima are interpreted to be caused by the three observed mm-thick volcanic ash layers with characteristic low resistivity values. The local maxima in gamma-ray counts marking the LPTM anomaly is dominated by large concentrations of thorium (rather than potassium or uranium), which supports a volcanic contribution to the claystone. These low-resistivity “ash peaks” of the FMS curve have counterparts in the GRAPE density, magnetic susceptibility, and iron intensity curves. The two minima in GRAPE density appear correlated to “Ash 3” and “Ash 1.” In the Fe intensity and magnetic susceptibility curves we identified all three ash layers: “Ash 3” is more pronounced in the Fe and “Ash 2” and “Ash 1” in the magnetic susceptibility curve. The fourth resistivity minima in the FMS resistivity curve at 975.75 mbsf may indicate a fourth ash layer, which is not lithologically apparent in the cores.

Site 1001

Downhole Measurements

Downhole measurements (note: geochemical data were not collected at Site 1001) reveal a relatively broad and less distinct anomaly compared to that observed at Site 999. The anomaly is best represented by a maximum in natural gamma-ray counts and minimum sonic velocity and FMS resistivity (Fig. 7) and is centered at ~240–241 mbsf.

The absolute minimum in FMS resistivity represented by the darkest area in the FMS image extends for only 9.2 cm, from 240.775 to 240.864 mbsf (Fig. 6). The broad anomaly in standard downhole logs is centered on this interval (~240.8 mbsf, Fig. 7).

The calibrated FMS resistivity curve displays distinctly different mean values below and above the anomaly (Fig. 7) and these trends extend uniformly for 10–15 m. In addition, the calibrated FMS resis-

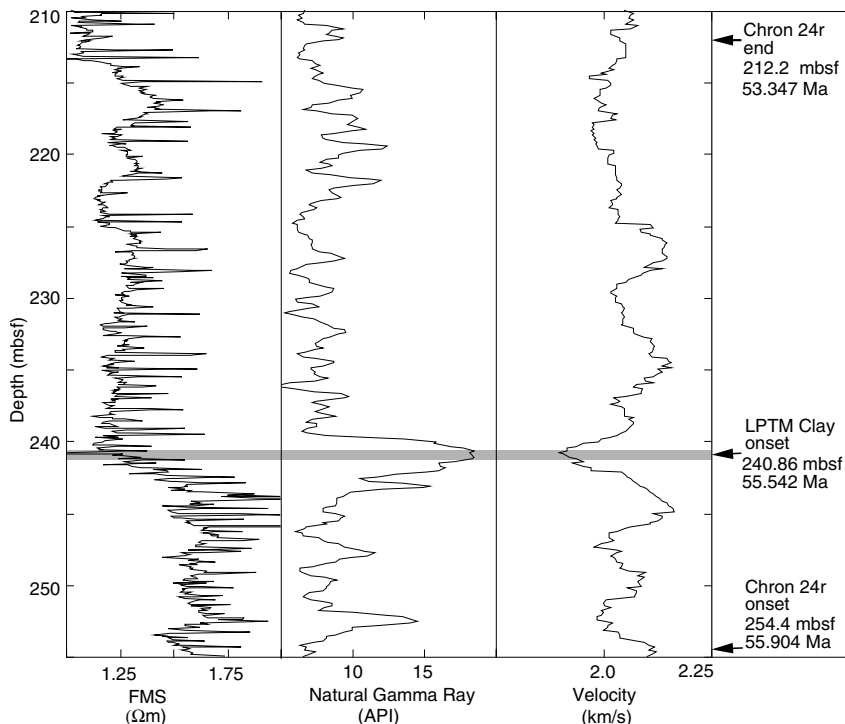


Figure 7. Late Paleocene thermal maximum (LPTM) as observed in selected downhole measurements at Site 1001. The log response at 240.8 mbsf is consistent with the recovered claystone interval that contains the negative $\delta^{13}\text{C}$ excursion marking the LPTM. The location of onset and termination of magnetochron C24r is also determined by downhole measurements (i.e., GHMT, V. Louvel and B. Galbrun, unpubl. data). The best estimate for the onset of the LPTM is 55.542 Ma, assuming a sedimentation rate of 37.4 m/m.y. based on nannofossil identification (Sigurdsson, Leckie, Acton, et al., 1997) and employing the Cande and Kent (1995) time scale. Note the distinct difference in resistivity above and below the LPTM and the short transition to lower resistivities prior to the LPTM.

tivity curve reveals a 3-m-long transition prior to the anomaly rather than post-LPTM as observed at Site 999 (Fig. 5).

Core Logs

The magnetic susceptibility and the calcium intensity curves for both LPTM Cores 165-1001A-27R and 165-1001B-6R are negatively correlated (Fig. 8). In general, the magnetic susceptibility values are relatively low, but some zones have magnetic susceptibility values up to 200 SI. The calcium intensities show a range from ~100 to 10,000 cps. The highest Ca intensity values found between 239.45 and 240.3 mbsf of Section 165-1001A-27R-3 could not be identified in Core 165-1001B-6R. The core data from 238.55 to 239.45 mbsf in Hole 1001A and 237.8 to 238.4 mbsf in Hole 1001B show generally low Ca intensities and higher susceptibility values.

Core Correlation and Core Log Integration

Core recovery at Site 1001 was considerably poorer than at Site 999 (54.7% in Hole 1001A, 66.8% in Hole 1001B). The cores covering the LPTM interval in Holes 1001A and 1001B are only 5.34 m (55% recovery) and 4.23 m long (44% recovery), respectively. The correlation of core data to downhole measurements is essential for reconstructing a single section from two adjacent cores in holes with such poor recovery. Reconstruction of a more complete section from Holes 1001A and 1001B was accomplished using FMS, core log data, and matching of distinguishing features, such as ash layers. Log-to-core correlations for the LPTM interval in particular are initiated by identifying log responses that distinguished the LPTM so clearly at Site 999.

The logging response in the upper Paleocene–lower Eocene portion of Hole 1001A can be interpreted in terms of the varying proportions of the primary constituents in the recovered samples (i.e., clay, chalk, chert, and varying amounts of volcanic ash) and to their relative porosities. The poor recovery is probably related to the generally higher frequency of lithologic alternations and the presence of chert interbedded with much less indurated material (i.e., clay rather than claystone, chalk rather than limestone). The magnetic susceptibility is generally low because of the relatively high carbonate content (up to 82.9%, Bralower et al., 1997), but the more clayey intervals, the LPTM clay, and altered volcanic ash horizons show magnetic susceptibility maxima. The wide variety of different lithologies ranging from pure limestones to pure claystones with transitional mixed sediment types is mirrored by the large range of Ca and Fe intensities and is apparent on the FMS image.

We identified characteristic altered volcanic ash or clay layers in the cores of the two holes both macroscopically and in detail by their typical magnetic susceptibility peak pattern; these horizons are labeled “D” to “P” in Figure 8 (same scheme as in Bralower et al., 1997). Some of these layers are up to several centimeters thick and can be used as index layers (e.g., the double peak “E,” the typically greenish ash layer “F,” and the “triple” “N1” to “N3” could be identified in both holes). But in detail and for the complete cores it was quite difficult to correlate core piece by core piece between the two holes. This was only possible using all the different data sets available. In Figure 9 the magnetic susceptibility curves are shown for Cores 165-1001A-27R and 165-1001B-6R. For correlation purposes we shifted the index layers “D,” “E,” “F,” “G,” and “N1” to “N3” to a common depth. The resulting gaps in core range from several cm to up to 90 cm (Fig. 9). Afterward, we examined the cores directly for potential gaps and drilling disturbances to make sure core sections could actually be missing at these positions.

The next step was to assign the resulting core and data pieces to the continuous FMS image and resistivity curve. The index clay/altered ash layers “E” to “K” and especially characteristic series of peaks (e.g., “E” to “G”) were used to identify corresponding index horizons in each hole using different physical and chemical parameters. Magnetic susceptibility and iron intensity show characteristic

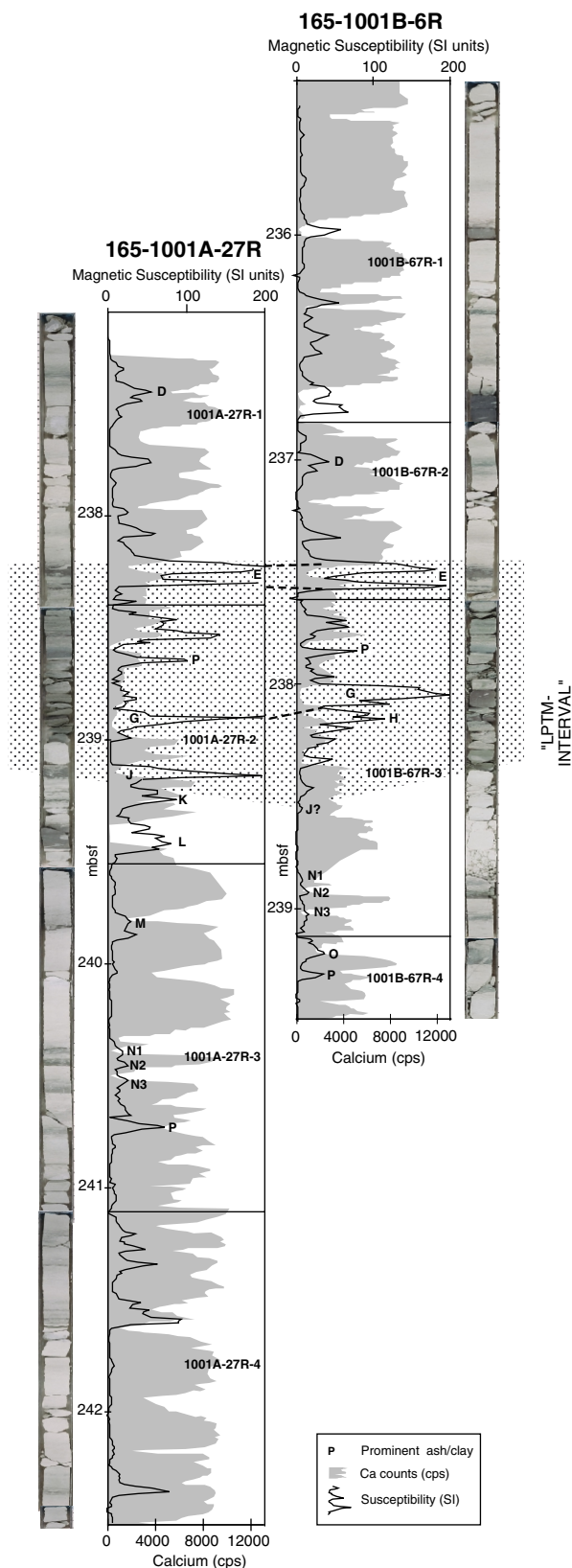


Figure 8. The Paleocene/Eocene boundary as observed in Cores 165-1001A-27R and 165-1001B-6R. Shown are the original drilling depths of the core and preliminary core correlations. The magnetic susceptibility measurements are collected at 1 cm intervals with the MSCL. For further explanation see text.

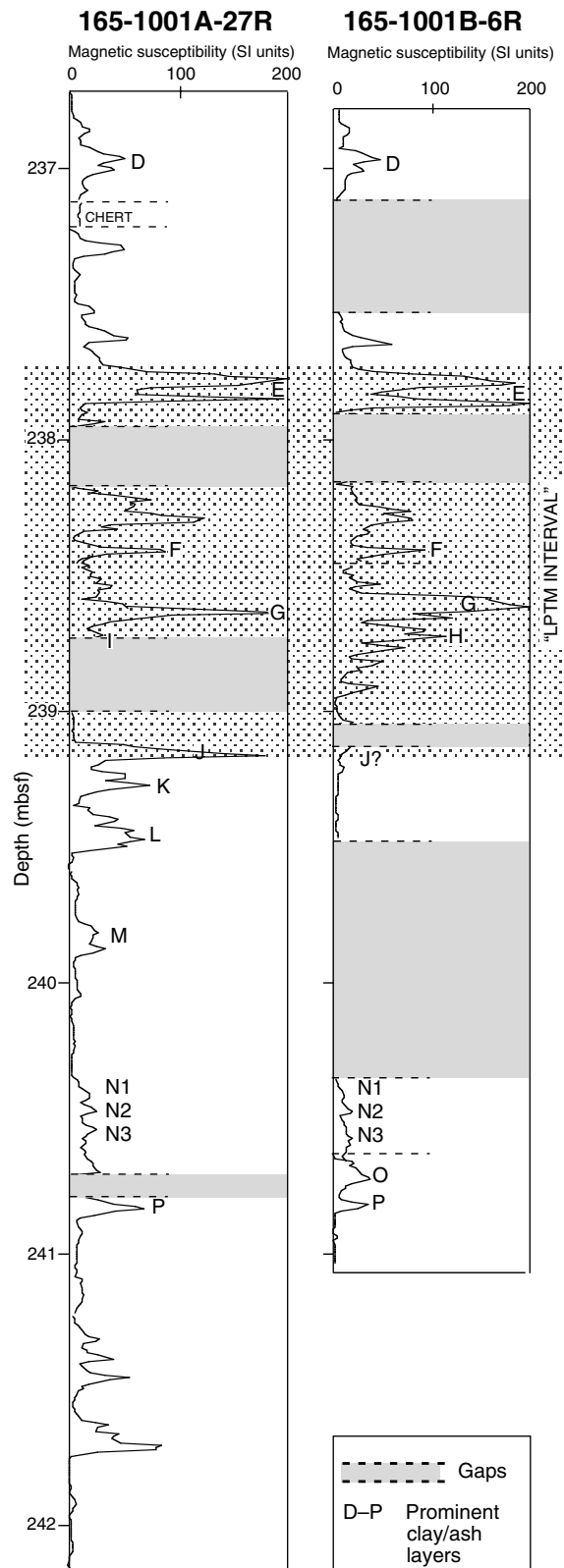


Figure 9. The Paleocene/Eocene boundary as observed in Cores 165-1001A-27R and 165-1001B-6R. The correlation of the two cores are shown: the core section data are partly cut into single pieces to allow better fit of the correlation and construction of a complete section. Magnetic susceptibility data are collected at 1 cm intervals with the MSCL.

maxima, and Ca intensity, GRAPE density, and FMS resistivity show distinct minima (Fig. 6). Carbonate-rich, high-resistivity layers were also used for correlating the core and downhole logs. This correlation indicates that the highest resistivity layers (very light gray to white) were not recovered. These horizons probably represent chert and/or silicified limestone layers.

In general there is a good correlation between Ca intensities and GRAPE densities. For example, in the upper part of the 4 m sections shown in Figure 6 (238–238.2 mbsf), where these two curves are almost parallel and just minor variations are found. This is different downhole (e.g., 240.55–240.8 mbsf), where single pronounced GRAPE density peaks have no equivalent within the Ca intensity curve. This pattern appears to be related to the presence of chert, characterized by high-resistivity values in these intervals. As soon as light gray to white colors in the FMS image (and therefore the chert layers) disappear, the Ca intensity and GRAPE density curves correlate quite well (e.g., 240.86–241.1 mbsf).

There is an overall good correlation between the magnetic susceptibility and iron intensity curves. The double peak “E” in the magnetic susceptibility curve (at ~238.3 mbsf) is irregular in the Fe intensity curve: the upper peak is more pronounced compared to the lower one. The LPTM clay shows a characteristic minimum in the FMS resistivity curve. The Fe intensity shows a differentiation of layer “I,” which is not visible in the magnetic susceptibility curve.

The anomaly in sonic velocity and gamma-ray counts is centered on the absolute minimum in FMS resistivity, which extends for only 9.2 cm (240.775–240.867 mbsf; Figs. 6, 7). The co-varying extreme logging values indicate a zone with relatively high clay content and low induration and are interpreted as a clay and/or claystone layer within chalk and mixed sedimentary rock with clay. The 60 cm (Hole 1001B) to 90 cm (Hole 1001A) thick intervals with generally low Ca intensities and higher magnetic susceptibility values are, as at Site 999, expected to contain the LPTM event. Shipboard biostratigraphy and the fortuitous recovery of a claystone unit containing a negative carbon isotope excursion (Bralower et al., 1997) locate the LPTM at ~239.5 mbsf (core depth) at the base of index layer “I” (Fig. 8, dotted region; Fig. 6). After the core composite was created as described above, the section of the core containing the $\delta^{13}\text{C}$ anomaly corresponded to the base of the LPTM clay at 240.86 mbsf as defined by the FMS image without any further depth shifting of the core. In other words, depth shifts and composite core construction were accomplished independently of matching the $\delta^{13}\text{C}$ anomaly to the FMS defined claystone, further supporting the interpretation of the FMS resistivity minimum as the LPTM clay. The extreme minimum $\delta^{13}\text{C}$ and uniformly low Ca intensities overlap the 9.2 cm FMS resistivity minimum and extend for a total of 30 cm, which we interpret as the LPTM clay thickness at Site 1001.

DISCUSSION

The LPTM log anomaly at Site 999 is abrupt and marks a distinct change in the physical and chemical properties of sediments above and below the LPTM anomaly (Fig. 4). The contrast in physical and chemical properties extends uniformly for 10–15 m above and below the LPTM claystone and indicates significant and long-term differences in the proportion of primary lithologies and their porosity across the LPTM. These observations are consistent with a rapid and extreme environmental change that persists beyond the LPTM anomaly itself. The LPTM log anomaly at Site 1001 does not appear as clear as that shown for Site 999; however, the FMS/SFLU resistivity values also indicate long-term differences in the physical properties of sediments above and below the anomaly. The LPTM interval is also characterized by a thin (short) interval of significantly lower Ca (i.e., carbonate) values, probably reflecting the shallowing of both the carbonate compensation depth (CCD) and the lysocline. Significant environmental changes are also documented by evidence for reduced

sea-floor ventilation (e.g., faint lamination, diminishing bioturbation; Sigurdsson, Leckie, Acton, et al., 1997; Bralower et al., 1997).

Downhole and core logging data thus support proposals that the LPTM claystone (log anomaly) is the product of a relatively short paleoceanographic event with an abrupt onset, followed by longer term changes in the ocean circulation that have been documented in contrasting sediment compositions in both low- and high-latitude sites (e.g., Kennett and Stott, 1991; Bralower et al., 1995; Thomas and Shackleton, 1996). At Site 999 there is no indication in the logging data of gradual changes preceding the LPTM that may have eventually crossed a threshold value resulting in the LPTM event. However, the FMS record at Site 1001 shows a 3-m transition from relatively high resistivities below the LPTM down to the local minimum resistivity value marking the LPTM, indicating that there is a gradual change in physical properties preceding the LPTM anomaly at this location (Fig. 7).

At Site 999, the abrupt onset of the FMS anomaly followed by a transition zone to higher values is similar to the pattern displayed by Ca and Fe intensities and magnetic susceptibility data (Figs. 4, 5); however, these lithologic indices return to their pre-LPTM levels within 1 m above the base of the LPTM, whereas FMS resistivities do not. Ca intensities decrease to a uniform minimum within 3 samples (i.e., 4 cm) indicating an onset time of less than a few thousand years (1.2 k.y. at a sedimentation rate of 32 m/m.y.) and is similar to C isotope patterns displayed by this and other sites worldwide (Bralower et al., 1997; Thomas and Shackleton, 1996).

The LPTM clay includes the negative $\delta^{13}\text{C}$ excursion, minimum values of Ca, Fe, and magnetic susceptibility, and is defined as 25 to 37 cm thick at Site 999. This clay is the base of a broader zone (97 cm thick) referred to as the LPTM "interval" defined by low resistivity, and the gradual return of Ca, Fe, magnetic susceptibility, and $\delta^{13}\text{C}$ to pre-LPTM levels. At Site 1001 the LPTM clay, including the characteristic FMS patterns observed at Site 999, correlates to index layer "I" and appears to be just 9.2 cm thick. However, the extreme $\delta^{13}\text{C}$ anomaly at Site 1001 is ~30 cm thick, which also matches the extent of constant minimum values in Ca, indicating that the LPTM clay is approximately 30 cm thick at this location. The LPTM interval at Site 1001 is 80-cm-thick and includes index layers "H" to "I" (Fig. 6). Thus thickness estimates for the LPTM interval and LPTM clay are comparable at these widely separated sites.

Our estimate of 97 cm for the LPTM interval and 37 cm (maximum) for the LPTM clay at Site 999 corresponds to approximately 30 k.y. and 11 k.y., respectively, assuming sedimentation rates of 32.2 m/m.y. calculated from nanofossil datums (Sigurdsson, Leckie, Acton, et al., 1997). A comparable calculation at Site 1001 indicates a duration of only 21 k.y. for the LPTM interval and 8 k.y. for the LPTM clay (i.e., 80 and 30 cm at 37.4 m/m.y.). These estimates are comparable to those based on species richness parameters and isotopic anomalies, which indicate the duration of the LPTM interval is on the order of 25 to 50 k.y. and that the event itself was in place in less than 10 k.y. (Thomas and Shackleton, 1996; Steineck and Thomas, 1996). The downhole log measurements, primarily at Site 999, indicate that this "short" event is followed by chemical/physical properties changes persisting for millions of years that is not evident in the isotope data. Downhole logging data also provide constraints on the onset time of the LPTM event. The geological high-sensitivity magnetic tool (GHMT) was used at Hole 1001A and a magnetic polarity reversal stratigraphy has been established (V. Louvel and B. Galbrun, unpubl. data). Analysis of GHMT data and conventional paleomagnetic analysis of cored samples indicate that Chron 24r extends from 254.4 to 212.2 mbsf (log depth), which corresponds to 55.904–53.347 Ma (V. Louvel and B. Galbrun, unpubl. data; Cande and Kent, 1995) (Fig. 4). The FMS image indicates the LPTM clay at Site 1001 begins at 240.867 mbsf. Assuming a Late Paleocene sedimentation rate of 37.4 m/m.y., based on nanofossil datums (Sigurdsson, Leckie, Acton, et al., 1997), the LPTM claystone appears abruptly at 55.54 Ma.

The occurrence of the LPTM at sometime early in C24r is consistent with other studies (e.g., Aubry et al., 1996; Berggren and Aubry, 1996), and the quantitative estimate of 55.54 Ma is similar to estimates made in recent studies (e.g., LPTM onset at 55.5 Ma; Thomas and Shackleton, 1996). This observation also provides further, independent support for the depth location of the LPTM based on downhole measurements. Unfortunately, GHMT was not used at Site 999, and it was not possible to obtain magnetostratigraphic data from the cores as the drilling overprint could not be removed (B. Galbrun, pers. comm., 1998).

Linear sedimentation rates used in this study are over estimated because they are calculated across distances (time intervals) that include the pronounced decrease in carbonate content which presumably reflects intense dissolution (i.e., an interval of lower sedimentation rate). Therefore our quantitative estimates of onset and duration times for the LPTM must be considered minimum values.

CONCLUSIONS

For the first time detailed downhole and core logging measurements have been made on lithologically variable, upper Paleocene, low-latitude sections containing the LPTM. Exact core-log integration is accomplished by detailed correlation of FMS data and continuous high-resolution core log data that allows the construction of a composite core from adjacent holes and correlation between two widely separated sites. The definition of composite sections was also essential for defining postcruise core sampling that verified the recovery of the LPTM by its characteristic negative shift in carbon isotope values.

The LPTM is identified by narrow (short term), co-varying anomalies in core logging data and continuous downhole measurements, which marks an abrupt, distinct, and long-term difference in physical and chemical properties of the strata above and below the LPTM.

With the exception of the FMS log at Site 1001, all downhole logs and high-resolution core logs show no evidence for gradual change preceding the LPTM, while above the LPTM the core-log data do show a gradual transition to pre-LPTM values.

The logging data alone support a multiphase LPTM, including a nearly instantaneous onset followed by a uniform, but very much altered, set of physical and chemical conditions of short duration referred to as the LPTM clay. The LPTM clay is succeeded by a longer transition to a new, more permanent environmental mode called the LPTM interval. The estimated duration of these "phases" relies on assumptions of sedimentation rates, and are consistent with paleontological and isotopic studies of the LPTM.

Whole-core high-resolution XRF data show that the LPTM interval is characterized by an abrupt shift to uniformly low Ca intensities (i.e., carbonate) which is interpreted to reflect a rapid shoaling of the CCD and lysocline. Ca intensities reach minimum values within 4 cm indicating an initiation of the LPTM of less than a few thousand years.

The minimum duration of the LPTM interval and LPTM clay defined by logging anomaly thicknesses and shipboard-derived sedimentation rates range from 21 to 30 k.y. and from 8 to 11 k.y., respectively.

The exact depth placement of the LPTM clay using FMS data coupled with polarity reversal stratigraphy from downhole measurements (V. Louvel and B. Galbrun, unpubl. data), and shipboard-derived sedimentation rates indicate an onset time for the LPTM early in C24r at 55.54 Ma.

The data indicate the presence of unrecovered, discrete ash layers within and surrounding the LPTM interval, which add to the already numerous recovered ash layers that define a late Paleocene–early Eocene pulse of explosive volcanism in the Caribbean region.

ACKNOWLEDGMENTS

We are grateful to the Ocean Drilling Program for inviting us to participate on Leg 165, to all members of the Shipboard Scientific Party of Leg 165 for their cooperation aboard the ship, and to the ODP personnel and the SEDCO crew who made Leg 165 a success. We especially thank Timothy J. Bralower, Veronique Louvel, and Bruno Galbrun for discussions and free data exchange. U.R acknowledges the financial support of the German Research Foundation (DFG), L.J.A. that of JOI-USSAC. We thank Aad Vaars, Bob Koster, and Sjerry Van der Gaast (Netherlands Institute for Sea Research, Texel, The Netherlands) for introducing us to the secrets of the XRF Core Scanner. We also thank the Borehole Research Group, LDEO, for postcruise data processing, and P. Pezard and V. Louvel for their assistance with FMS-SFLU calibration at the *Laboratoire de Mesures en Forage*, Marseille, France. Valuable reviews and critiques were provided by Espen Sletten Andersen, Timothy J. Bralower, and Julie A. Hood.

REFERENCES

- Aubry, M.-P., Berggren, W.A., Stott, L., and Sinha, A., 1996. The upper Paleocene–lower Eocene stratigraphic record and the Paleocene/Eocene boundary carbon isotope excursion: implications for geochronology. *In* Knox, R.W.O'B., Corfield, R.M., and Dunay, R.E. (Eds.), *Correlation of the Early Paleogene in Northwestern Europe*. Spec. Publ.—Geol. Soc. Am., 101:353–380.
- Berggren, W.A., and Aubry, M.-P., 1996. A late Paleocene–early Eocene NW European and North Sea magnetobiochronological correlation network. *In* Knox, R.W.O'B., Corfield, R.M., and Dunay, R.E. (Eds.), *Correlation of the Early Paleogene in Northwest Europe*. Spec. Publ.—Geol. Soc. Am., 101:309–352.
- Borehole Research Group, 1990. *Ocean Drilling Program Logging Manual*, LDEO.
- Bourke, L., Delfiner, P., Trouiller, J.-C., Fett, T., Grace, M., Luthi, S., Serra, O., and Standen, E., 1989. Using Formation MicroScanner images. *Tech. Rev.*, 37:16–40.
- Boyce, R.E., 1976. Definitions and laboratory techniques of compressional sound velocity parameters and wet-water content, wet-bulk density, and porosity parameters by gravimetric and gamma-ray attenuation techniques. *In* Schlanger, S.O., Jackson, E.D., et al., *Init. Repts. DSDP*, 33: Washington (U.S. Govt. Printing Office), 931–958.
- Bralower, T.J., Thomas, D.J., Zachos, J.C., Hirschmann, M.M., Röhl, U., Sigurdsson, H., Thomas, E., and Whitney, D.L., 1997. High-resolution records of the late Paleocene thermal maximum and circum-Caribbean volcanism: is there a causal link? *Geology*, 25:963–966.
- Bralower, T.J., Zachos, J.C., Thomas, E., Parrow, M., Paull, C.K., Kelly, D.C., Premoli Silva, I., Sliter, W.V., and Lohmann, K.C., 1995. Late Paleocene to Eocene paleoceanography of the equatorial Pacific Ocean: stable isotopes recorded at Ocean Drilling Program Site 865, Allison Guyot. *Paleoceanography*, 10:841–865.
- Cande, S.C., and Kent, D.V., 1995. Revised calibration of the geomagnetic polarity timescale for the Late Cretaceous and Cenozoic. *J. Geophys. Res.*, 100:6093–6095.
- Curry, W.B., Shackleton, N.J., Richter, C., et al., 1995. *Proc. ODP, Init. Repts.*, 154: College Station, TX (Ocean Drilling Program).
- deMenocal, P.B., Bristow, J.F., and Stein, R., 1992. Paleoclimatic applications of downhole logs: Pliocene–Pleistocene results from Hole 798B, Sea of Japan. *In* Pisciotto, K.A., Ingle, J.C., Jr., von Breymann, M.T., Barron, J., et al., *Proc. ODP, Sci. Results*, 127/128 (Pt. 1): College Station, TX (Ocean Drilling Program), 393–406.
- Dickens, G.R., Castillo, M.M., and Walker, J.G.C., 1997. A blast of gas in the latest Paleocene: simulating first-order effects of massive dissociation of oceanic methane hydrate. *Geology*, 25:259–262.
- Dickens, G.R., O'Neil, J.R., Rea, D.K., and Owen, R.M., 1995. Dissociation of oceanic methane hydrate as a cause of the carbon isotope excursion at the end of the Paleocene. *Paleoceanography*, 10:965–971.
- Ekstrom, M.P., Dahan, C.A., Chen, M.-Y., Lloyd, P.M., and Rossi, D.J., 1986. Formation imaging with microelectrical scanning arrays. *Trans. SPWLA 27th Annu. Logging Symp.*, Pap. BB.
- Eldholm, O., and Thomas, E., 1993. Environmental impact of volcanic margin formation. *Earth Planet. Sci. Lett.*, 117:319–329.
- Gunn, D.E., and Best, A.I., 1998. A new automated nondestructive system for high resolution multi-sensor core logging of open sediment cores. *Geo-Mar. Lett.*, 18:70–77.
- Jansen, J.H.F., Van der Gaast, S.J., Koster, B., and Vaars, A.J., 1998. COR-TEX, a shipboard XRF-scanner for element analyses in split sediment cores. *Mar. Geol.*, 151:143–153.
- Kennett, J.P., and Stott, L.D., 1990. Proteus and Proto-oceanus: ancestral Paleogene oceans as revealed from Antarctic stable isotopic results: ODP Leg 113. *In* Barker, P.F., Kennett, J.P., et al., *Proc. ODP, Sci. Results*, 113: College Station, TX (Ocean Drilling Program), 865–880.
- , 1991. Abrupt deep-sea warming, paleoceanographic changes and benthic extinctions at the end of the Paleocene. *Nature*, 353:225–229.
- Knox, R.W.O'B., 1996. Correlation of the early Paleogene in northwest Europe: an overview. *In* Knox, R.W.O'B., Corfield, R.M., and Dunay, R.E. (Eds.), *Correlation of the Early Paleogene in Northwest Europe*. *Geol. Soc. Spec. Publ. London*, 101:1–11.
- Neal, J.E., 1996. A summary of Paleogene sequence stratigraphy in northwest Europe and the North Sea. *In* Knox, R.W., Corfield, R.M., Dunay, R.E. (Eds.), *Correlation of the Early Paleogene in Northwest Europe*. *Geol. Soc. Spec. Publ. London*, 101:15–42.
- Norris, R.D., Kroon, D., Klaus, A., et al., 1998. *Proc. ODP, Init. Repts.*, 171B: College Station, TX (Ocean Drilling Program).
- Pak, D.K., and Miller, K.G., 1992. Paleocene to Eocene benthic foraminiferal isotopes and assemblages: implications for deepwater circulation. *Paleoceanography*, 7:405–422.
- Pindell, J.L., and Barrett, S.F., 1990. Geologic evolution of the Caribbean region: a plate-tectonic perspective. *In* Dengo, G., and Case, J.E. (Eds.), *The Caribbean Region*. *Geol. Soc. Am., Geol. North. Am. Ser.*, H:405–432.
- Shackleton, N., and Boersma, A., 1981. The climate of the Eocene ocean. *J. Geol. Soc. London*, 138:153–157.
- Shackleton, N.J., 1986. Paleogene stable isotope events. *Palaeogeogr., Palaeoclimatol., Palaeoecol.*, 57:91–102.
- Sigurdsson, H., Leckie, R.M., Acton, G.D., et al., 1997. *Proc. ODP, Init. Repts.*, 165: College Station, TX (Ocean Drilling Program).
- Steinbeck, L.P., and Thomas, E., 1996. The latest Paleocene crises in the deep sea: ostracode succession at Maud Rise, Southern Ocean. *Geology*, 24:583–586.
- Thomas, E., and Shackleton, N., 1996. The Palaeocene–Eocene benthic foraminiferal extinction and stable isotope anomalies. *In* Knox, R.W.O'B., Corfield, R.M., and Dunay, R.E. (Eds.), *Correlation of the Early Paleogene in Northwest Europe*. *Geol. Soc. Spec. Publ. London*, 101:401–441.
- Weaver, P.P.E., and Schultheiss, P.J., 1990. Current methods for obtaining, logging, and splitting marine sediment cores. *Mar. Geophys. Res.*, 12:85–100.
- Wessel, P., and Smith, W.H.F., 1995. New version of the Generic Mapping Tools released. *Eos*, 76:329.
- Zachos, J.C., Lohmann, K.C., Walker, J.C.G., and Wise, S.W., Jr., 1993. Abrupt climate change and transient climates during the Paleogene: a marine perspective. *J. Geol.*, 101:191–213.
- Zachos, J.C., Rea, D.K., Seto, K., Niitsuma, N., and Nomura, R., 1992. Paleogene and early Neogene deep water history of the Indian Ocean: inferences from stable isotopic records. *In* Duncan, R.A., Rea, D.K., Kidd, R.B., von Rad, U. and Weissel, J.K. (Eds.), *The Indian Ocean: A Synthesis of Results from the Ocean Drilling Program*. *Am. Geophys. Union, Geophys. Monogr.*, 70:351–386.

Date of initial receipt: 29 June 1998

Date of acceptance: 3 March 1999

Ms 165SR-009